World Conference on
Timber Engineering
Oslo 2023

NUMERICAL HOMOGENISATION OF MECHANICAL PROPERTIES OF PINUS PINASTER (AIT.) LAMELLAE CONSTITUTING GLUED LAMINATED TIMBER

Romain Chevalier[1], Bruno Vuillod[2], Mathilde Zani[3], Marco Montemurro[4], Régis Pommier[5], Anita Catapano[6]

ABSTRACT:

Pinus pinaster (Ait.) is a softwood species considerably employed in the current wood industry in the Southwest of France. In a context of new environmental constraints, describing and predicting the behaviour of this local species becomes a matter of high priority. Nonetheless, the vast majority of industrial and research works still use classical softwood properties to determine various engineered Pinus pinaster (Ait.) products characteristics such as glued laminated and cross laminated timber.

This work proposes to employ general numerical homogenisation techniques used in the field of composite materials to obtain mechanical properties of Pinus pinaster (Ait.) as well as wood products such as glued laminated timber (Glulam). The proposed approach consists in decomposing and modelling glued laminated timber in four working scales: scale of glulam products, lamellae of several typologies composing such wood products (macroscopic scale), wood volumes considered analogous to laminar composites (mesoscopic scale) and composed of a few growth rings (microscopic scale) of initial and final wood. The homogenisation technique, adopted to compute properties from the microscopic to the macroscopic scale, is combined with approximation methods reposing on non-uniform rational basis spline entities to compute the mechanical properties of lamellae constituting glulam.

KEYWORDS: Numerical Homogenisation, Approximation methods, Pinus pinaster (Ait.), Glulam, Composite Materials

[1] Romain Chevalier, **Université de Bordeaux**, **Gascogne Bois**, Arts et Métiers Institute of Technology, Bordeaux INP, CNRS, INRA, HESAM Université, I2M UMR 5295, F-33400 Talence, France, romain.chevalier@ensam.eu
[2] Bruno Vuillod, **French Atomic Energy Commission**, Route des Gargails, BP2, Le Barp Cedex, FranceArts et Metiers Institute of Technology, Univ. Bordeaux, CNRS, Bordeaux INP, Hesam Universite, I2M, UMR 5295, F-33400 Talence, France, bruno.vuillod@ensam.eu
[3] Mathilde Zani, **Arts et Métiers Institute of Technology**, Université de Bordeaux, CNRS, INRA, Bordeaux INP, HESAM Université, I2M UMR 5295, F-33400 Talence, France, mathilde.zani@ensam.eu
[4] Marco Montemurro, **Arts et Métiers Institute of Technology**, Université de Bordeaux, CNRS, INRA, Bordeaux INP, HESAM Université, I2M UMR 5295, F-33400 Talence, France, marco.montemurro@ensam.eu
[5] Régis Pommier, **Université de Bordeaux**, Arts et Métiers Institute of Technology, Bordeaux INP, CNRS, INRA, HESAM Université, I2M UMR 5295, F-33400 Talence, France, regis.pommier@u-bordeaux.fr
[6] Anita Catapano, **Bordeaux INP**, Université de Bordeaux, Arts et Métiers Institute of Technology, CNRS, INRA, HESAM Université, I2M UMR 5295, F-33400 Talence, France, anita.catapano@bordeaux-inp.fr

https://doi.org/10.52202/069179-0062

1 INTRODUCTION

Wood is a natural material whose importance has risen exponentially over the last few years. Indeed, this renewable material perfectly fits several "Sustainable Development Goals" set by the United Nations and is highly recommended by the IPCC's "Global Warming of 1.5°C" report [1] as a solution to reduce carbon footprints in building and civil-engineering. In the South West of France, the current wood industry (including the company Gascogne Bois (GB)) is particularly related to Pinus pinaster (Ait.), a softwood species indigenous of the South West of Europe, because of its vast presence across the whole area (between 75% to 84% of total forest area in two French departments [2]).

Glued laminated timber (glulam) is a wood product manufactured by gluing and finger-jointing multiple wood lamellae allowing flexibility in size and shape. Furthermore, wood distortions issued from thermo-hygric variations can be considerably reduced in glulam by assembling a disparity of lamellae properties [3]. This advantage is noticeably reduced when using Pinus pinaster (Ait.) timber. Several studies [4,5] tried to estimate the shape stability of multiple configurations of softwoods glulam. However, the vast majority of studies are focused on others softwood species or use classical softwood properties taken from [6]. Moreover, the variability of wood properties are also neglected.

Hence, the main purpose of this work is to propose a multi-scale mechanical model of lamellae constituting glulam able to take into account the physical properties and related variability of Pinus pinaster (Ait.).

The paper is organiser as follows : modelling of physical and mechanical properties of the two phases of initial and final wood constituting growth rings is presented in Section 2. Section 3 is dedicated to the description of the numerical homogenisation procedure of the mechanical properties of elementary volumes of Pinus pinaster (Ait.). The results of the numerical study is presented in Section 4. Approximation methods are then used to compute the properties of multiple typologies of lamellae in Section 5. Finally, conclusions and perspectives are dispensed in Section 6.

2 PINUS PINASTER (AIT.) STRUCTURE AND PROPERTIES

2.1 MULTI-SCALE DEFINITION

Wood is a highly heterogeneous and anisotropic natural composite whose structure can be defined at three working scales:

- Growth ring composed by the accumulation of wood cells (90% of longitudinal tracheids) at the microscopic scale.
- Elementary volume emerging from the alternation of a few initial wood (IW) and final wood (FW) growth rings at the mesoscopic scale considered as lamellar composite.
- Wood lamellae formed by the combination of elementary volumes of multiple growth ring patterns at the macroscopic scale.

2.2 MODELLING OF PINUS PINASTER (AIT.) LOG

A local orthotropic coordinate system is used to describe wood properties defined by three preferred directions according to Figure 1: longitudinal direction L, radial direction R corresponding to the diametrical growth direction, and tangential direction T to the annual growth rings. Three planes can be identified in this system: the transverse plane RT, the radial longitudinal plane LR and the tangential longitudinal plane LT.

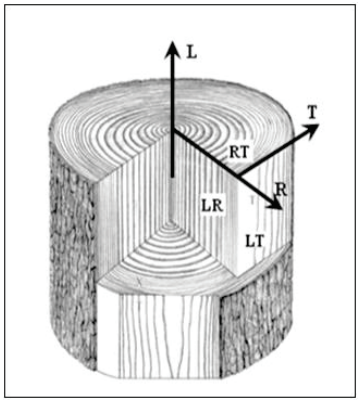

Figure 1: *Local reference system [7]*

The proposed model takes into consideration the difference between initial and final wood and the difference between juvenile and adult wood for growth rings from pith to bark.

Tree trunks are considered straight, with concentric growth rings, centred pith, and a circular shape of the transversal section (plane RT) across the whole L direction. Heartwood formation (no real influence on mechanical properties [8]), presence of knots, and reaction wood are neglected. Grain angle is considered null.

As for the physical properties, ring widths RW, mean relative density d, mean FW relative density FWd, and final wood proportion FWp (proportion of FW in a ring) are regarded at each ring number i. Globally, their variation is considered as function of the distance from the

https://doi.org/10.52202/069179-0062

pith R. Their dependency to the height H is neglected. Variability of such properties is considered at every growth ring. Properties are considered constant in the adult wood, which begins at the 15th ring (juvenile-adult wood limit at 12 years old [9] in the case of Pinus pinaster (Ait.)).

The physical properties relative to ring number i for our Pinus pinaster (Ait.) model are presented in Table 1. They are qualitatively extracted from several references [9,10,11]. The RW properties are adapted to match the data of GB company. Regarding FWp, d, and FWd, their evolution is considered linear with ring number in the juvenile wood and constant in the adult wood.

Table 1: *Physical properties for the Pinus pinaster (Ait) model.*

Ring N° i	RW [mm]	FWp [%]	d	FWd
1	2.5	8	0.43	0.56
2	9.4	10	0.439	0.57
3	10.0	12	0.447	0.58
4	10.2	14	0.456	0.59
5	10.1	16	0.464	0.60
6	9.9	18	0.473	0.61
7	9.0	20	0.481	0.62
8	7.8	22	0.490	0.63
9	6.5	24	0.499	0.64
10	5.3	26	0.507	0.65
11	4.3	28	0.516	0.66
12	3.4	30	0.524	0.67
13	2.8	32	0.533	0.68
14	2.3	34	0.541	0.69
15	2	36	0.55	0.70

In analogy to [12] in the case of a natural material, wood properties defined in this study are governed by uncertainty and their variability is described by a normal distribution at each ring number i (except the first three rings considered constant because of the lack of information in the scientific literature). For a generic property q_i, Equation (1) describes the normal probability density function $\psi(q_i)$ with $\lambda(q_i)$ and $\xi(q_i)$, respectively, the mean value and the standard deviation of the distribution of the property q_i:

$$\psi(q_i) = \frac{1}{\xi(q_i)\sqrt{2\pi}} exp\left(-\frac{\left(q_i - \lambda(q_i)\right)^2}{2\xi(q_i)^2}\right). \quad (1)$$

The mean value $\lambda(q_i)$, standard deviation $\xi(q_i)$, and coefficient of variation $C_v(q_i)$ [%] can be expressed as follows :

$$\lambda(q_i) = \frac{1}{N_v}\sum_{j=1}^{N_v} q_{i,j}\ ,$$
$$\xi(q_i) = \sqrt{\lambda\left(\left(q_i - \lambda(q_i)\right)^2\right)}, \quad (2)$$
$$C_v(q_i) = 100\frac{\xi(q_i)}{\lambda(q_i)}\ ,$$

where $q_{i,j}$ is the jth value of q_i occurring for N_v values :

Regarding the RW and the FWp, the coefficient of variation at each ring number is considered equal to 20% as to be in the same order of magnitude as the references in the scientific literature [11,13]. In the case of d and FWd, a hypothesis is made to consider the wood mass produced by a ring as constant. Hence, a modification of RW and FWp induce a variation of the densities values d and FWd.

The number of ring is defined by the age of the trees considered. In the Landes of Gascogne, 92% of the local forest is private property. Hence, traceability of stands processed by GB company is not ensured and tree ages are unknown.

Nonetheless, GB company possesses dendrological data on the mean and standard deviation of log diameter evaluated on 149727 logs. The measurements were performed for logs of 2.5m extracted between 0m-8m. (Note: GB standard deviation results are overvalued because referenced as 120 stacks of 2500 tree). Few information exists on the trees treated by GB including a minimal age of 40 years old and the possibility to reach 60 years old.

Our model has to take into consideration the heterogeneity of tree ages resulting in a varying number of rings relative to match the GB data. To this end, a hypothesis is introduced : in the following of this paper a half normal distribution with a mean age of 40 and a standard deviation of 7.5 admitting that age cannot be less than 40 years (99% of the ages are included between 40 and 62 years old) is considered. The mean diameter and standard deviation for the GB sample and for the numerical model, performed on a sample of 500 simulations, are presented in Table 2.

Table 2: *Mean diameter and standard deviation for wood logs taken from GB data and the parametric model.*

	GB sample	Parametric Model
Mean diameter [mm]	313.1	314.2
Standard deviation [mm]	19.15	20.34

2.3 ELASTIC PROPERTIES OF INITIAL AND FINAL WOODS AT THE MICROSCPIC SCALE

IW and FW elastic behaviour can be modelled at the microscopic scale through Hooke's law whose compliance matrix for wood is uniquely defined via 9 independent elastic constants: three Young's moduli E_m (m = L,R,T), three shear moduli G_{mn} (m,n = L,R,T and $m \neq n$), and three Poisson's ratios υ_{mn} (m,n = L,R,T and $m \neq n$):

https://doi.org/10.52202/069179-0062

$$\begin{Bmatrix} \varepsilon_L \\ \varepsilon_R \\ \varepsilon_T \\ \gamma_{LR} \\ \gamma_{TL} \\ \gamma_{RT} \end{Bmatrix} = \begin{bmatrix} \frac{1}{E_L} & -\frac{\upsilon_{RL}}{E_R} & -\frac{\upsilon_{TL}}{E_T} & 0 & 0 & 0 \\ -\frac{\upsilon_{LR}}{E_L} & \frac{1}{E_R} & -\frac{\upsilon_{TR}}{E_T} & 0 & 0 & 0 \\ -\frac{\upsilon_{LT}}{E_L} & -\frac{\upsilon_{RT}}{E_R} & \frac{1}{E_T} & 0 & 0 & 0 \\ 0 & 0 & 0 & \frac{1}{G_{LR}} & 0 & 0 \\ 0 & 0 & 0 & 0 & \frac{1}{G_{TL}} & 0 \\ 0 & 0 & 0 & 0 & 0 & \frac{1}{G_{RT}} \end{bmatrix} \begin{Bmatrix} \sigma_L \\ \sigma_R \\ \sigma_T \\ \tau_{LR} \\ \tau_{TL} \\ \tau_{RT} \end{Bmatrix} \quad (3)$$

where ε_m and σ_m are the normal strain and stress, respectively, along m-th axis, whilst γ_{mn} and τ_{mn} are the shear strain and stress, respectively, in the mn plane.

In the scientific literature, wood elastic properties can be expressed as a linear function of the relative density [14]. In [6], the authors proposed a linear model to compute softwoods elastic properties based on experimental results on a large variety of softwood species which is frequently used in most studies. Nonetheless, this model is fairly accurate for lower relative densities; it looses in precision in the case of high density softwood such as Pinus pinaster (Ait.), whereas the model proposed in this paper takes into consideration a FW phase of high relative density.
In this study, we propose to employ data relative to Pinus pinaster (Ait.) mechanical properties taken from the scientific literature [15,16,17,18,19] to establish elastic laws accurately describing the behaviour of IW and FW relative to this softwood species while taking into consideration the dependency to density. To this end, we also admit a linear relationship of the Young's and shear moduli with relative density similarly to the one presented in [6]. Regarding the Poisson's ratios, there is not enough information in the case of Pinus pinaster (Ait.) and their values are considered constant.

2.3.1 Young's moduli

In the case of the trend of the longitudinal Young's modulus with the relative density, eight values were provided in [15], which are reported in Table 3.

Table 3: *Mean longitudinal Young's modulus and density obtained through flexural tests in [15]*

d	0.46	0.60	0.635	0.64	0.65	0.693	0.705	0.715
E_L [GPa]	13.2	15.7	16.11	16.6	16.435	16.794	17.775	17.1

A linear relationship between the mean longitudinal modulus E_L [MPa] and mean relative density d is found and is described in Equation 4 with a coefficient of determination of ${R_d}^2 = 0.9581$.

$$E_L = 5875 + 16209\, d\,. \quad (4)$$

Three references, [16,17,18], estimated Young's moduli but omitting the relative density of the specimens. By considering a similar behaviour in traction and compression from wood samples, the linear relationship Equation (4) allows to estimate the density of the samples from the above studies. The densities estimations and the elastic properties are displayed in Table 4.

Table 4: *Mean Young's moduli and with estimated relative densities from [16,17,18].*

	E_L	E_R	E_T	d
Cariou [16]	11369	/	703	0.3390
Pereira et al. [17]	15100	1910	1010	0.5690
Lahna [18]	16140	2086	/	0.6439

Thus, it is now possible to propose linear relationship with associated density d_k associated to the phase k =IW,FW for the three Young's moduli that are presented in Equation (5):

$$\begin{aligned} E_{L_k} &= 16209\, d_k + 5874.7, \\ E_{R_k} &= 2972.2\, d_k + 238.70, \\ E_{T_k} &= 1334.8\, d_k + 250.51, \end{aligned} \quad (5)$$

with E_{L_k}, E_{R_k}, and E_{T_k} the Young's moduli associated to the phase k = IW,FW.

2.3.2 Shear moduli

[19] characterised the shear moduli of Pinus pinaster (Ait.) by carrying out two shear test methods (Iosipescu and off-axis). Equation (6) presents the models proposed to link shear moduli in [MPa] with infra-density (IF) [20]. They are considered applicable on the densities examined in our study.

$$\begin{aligned} G_{RT_k} &= 495\, IF_k, \\ G_{TL_k} &= 2072\, IF_k, \\ G_{LR_k} &= 2402\, IF_k, \end{aligned} \quad (6)$$

where $IF_k = \frac{d_k}{1.12+0.159\, d_k}$, G_{RT_k}, G_{TL_k}, and G_{LR_k}, respectively, with k = IW,FW.

2.3.3 Poisson's ratios

In [16], the author characterised the elastic properties of Pinus pinaster (Ait.) thanks to experimental tests. Table 5 presents the Poisson's ratio obtained in [16]. As there is too few information in the literature about the variation of Poisson's ratios as a function of the relative density, the ratios υ_{RT_k}, υ_{TL_k}, and υ_{RL_k}, are considered constant for the two phases k = IW,FW.

Table 5: *Pinus pinaster (Ait.) Poisson's ratio, [16] with k=IW,FW.*

υ_{RT_k}	υ_{TL_k}	υ_{RL_k}
0.58	0.03	0.04

2.3.4 Validity of the model

It is necessary to check the conformity of the model with respect to the true wood behaviour. In [6,16], the authors expressed the plausibility for several ratios between elastic properties to be quasi-constant such as E_{L_k}/E_{T_k}, E_{L_k}/E_{R_k}, G_{LR_k}/G_{RT_k}, and G_{TL_k}/G_{LR_k}. In this study, a ratio is considered quasi-constant if the maximum precentage difference between the properties computed over the density range [0.40,0.80] with the mean property computed at the relative density of 0.55 is lower than 10%. All ratios are considered quasi-constant as the condition aforementioned is fulfilled. Furthermore, the positive definiteness of the stiffness tensors is verified for the whole density range.

3 DETERMINATION OF THE ELASTIC PROPERTIES AT THE MESOSCOPIC SCALE

At the microscopic scale, the bibliographic data and the multiple hypotheses done on the properties of Pinus pinaster (Ait.) allow to propose two different material models for both initial and final woods taking into consideration their variability into the stem according to their corresponding relative density.

At the mesoscopic scale, the representative volume element (RVE), which can be seen as a lamellar composite, is modelled by an alternation of growth rings composed by both initial and final wood of varying width. The well-known numerical homogenisation method based on the strain energy of periodic media [21] is then employed to compute the mechanical properties of 3D cubic FE-model of the RVE of wood specimens extracted from several positions in the modelled logs of Pinus pinaster (Ait.).

This technique is based on the use of periodic boundary conditions (PBCs) to calculate the equivalent stiffness matrix of the material at the mesoscopic scale. However, PBCs cannot be applied directly to the lamellae at the mesoscopic scale because of growth ring patterns. Hence, lamellae are separated into several elementary cubes of relatively small dimensions to consider growth rings as rectangular parallelepipeds and to apply the homogenisation technique.

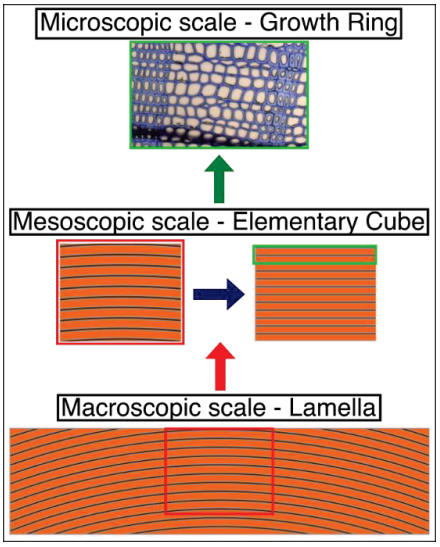

Figure 2 : *Multi-scale modelling of Pinus pinaster (Ait.) Glulam (Microscopic scale image adapted from [22])*

To consider the growth rings as rectangular parallelepipeds, a trigonometric study is realised on the elementary volumes considered as cubes of dimension h. The condition will be fulfilled over the whole range R ∈ [0;150]mm if the dimension h respects the following inequality h≤ 12mm.

The homogenisation procedure will then be coupled with a stochastic approach, the Monte-Carlo method, to efficiently compute the mesoscopic properties impacted by the overall variability.

The following assumptions are made to determine the effective properties at the mesoscopic scale:

- linear orthotropic behaviour defined in a local cylindrical reference system for all phases of initial and final wood;
- perfect bonding condition at the phases interface is considered.

3.1 The numerical homogenisation method

The geometry used for the RVE is the one depicted in Figure 2 with a cube considered as a lamellar composite. The geometric variable parameters used are the dimension of the cube h, the position of the centroid of the RVE R, the properties of the rectangular parallelepiped approximating the growth rings RW and FWp depending on the distance to the pith. The volume of the RVE is defined in Equation (7) in a local Cartesian reference system (O; x_1, x_2, x_3) defined at the centre of the RVE, with a_1, a_2, and a_3 the length of the RVE sides along the x_1, x_2, and x_3 axis, respectively.

$$V_{\text{RVE}} = a_1\, a_2\, a_3 \; = h^3. \tag{7}$$

The generation of synthetic logs is first coded in Python® environment. The parametric FE-model is then created within the commercial FE code Ansys®. 20-node solid elements SOLID186 with three Degree of Freedom

https://doi.org/10.52202/069179-0062

(DOF) per node have been used. The "Layered" element option has been selected to create and mesh only the RVE volume and model each ring as an equivalent layered section with 3 integration points per layer. In the 3D case, the generalised Hooke's law for the equivalent elastic material corresponding to the RVE can be written as:

$$\begin{Bmatrix} \bar{\sigma}_1 \\ \bar{\sigma}_2 \\ \bar{\sigma}_3 \\ \bar{\sigma}_4 \\ \bar{\sigma}_5 \\ \bar{\sigma}_6 \end{Bmatrix} = \begin{bmatrix} \bar{C}_{11} & \bar{C}_{12} & \bar{C}_{13} & \bar{C}_{14} & \bar{C}_{15} & \bar{C}_{16} \\ \bar{C}_{21} & \bar{C}_{22} & \bar{C}_{23} & \bar{C}_{24} & \bar{C}_{25} & \bar{C}_{26} \\ \bar{C}_{31} & \bar{C}_{32} & \bar{C}_{33} & \bar{C}_{34} & \bar{C}_{35} & \bar{C}_{36} \\ \bar{C}_{41} & \bar{C}_{42} & \bar{C}_{43} & \bar{C}_{44} & \bar{C}_{45} & \bar{C}_{46} \\ \bar{C}_{51} & \bar{C}_{52} & \bar{C}_{53} & \bar{C}_{54} & \bar{C}_{55} & \bar{C}_{56} \\ \bar{C}_{61} & \bar{C}_{62} & \bar{C}_{63} & \bar{C}_{64} & \bar{C}_{65} & \bar{C}_{66} \end{bmatrix} \begin{Bmatrix} \bar{\varepsilon}_1 \\ \bar{\varepsilon}_2 \\ \bar{\varepsilon}_3 \\ \bar{\varepsilon}_4 \\ \bar{\varepsilon}_5 \\ \bar{\varepsilon}_6 \end{Bmatrix}, \quad (8)$$

where $\bar{\sigma}$ and $\bar{\varepsilon}$ are the stress and strain tensors expressed in Voigt's notation, respectively associated with the equivalent homogeneous solid and as such are volume averaged, see [23] for more details.
The goal of this method is to evaluate all the components of the stiffness tensor $\bar{\mathbf{C}}$ by applying successively 6 load cases to the cubic RVE through classical PBCs [21].

After determining the components of the volume-averaged stress tensor (according to the procedure presented in [23]), the components of the elasticity matrix at the mesoscopic scale are calculated, for each set of PBCs, as:

$$\bar{C}_{\alpha\beta} = \frac{\bar{\sigma}_\alpha}{\bar{\varepsilon}_\beta} \text{ with } \beta = 1,2,\dots,6, \quad (9)$$

and $\bar{\varepsilon}_\gamma = 0$, with $\gamma = 1,2,\dots,6$ and $\gamma \neq \beta$.

Furthermore, it is possible to evaluate the effective elastic moduli of the composite material from the compliance tensor $\bar{\mathbf{S}} = \bar{\mathbf{C}}^{-1}$, as shown below [23].

Three Young's moduli:

$$E_1 = \frac{1}{\bar{s}_{11}}, E_2 = \frac{1}{\bar{s}_{22}}, E_3 = \frac{1}{\bar{s}_{33}}.$$

Three shear moduli:

$$G_{23} = \frac{1}{\bar{s}_{44}}, G_{13} = \frac{1}{\bar{s}_{55}}, G_{12} = \frac{1}{\bar{s}_{66}}.$$

Three Poisson's ratios:

$$\upsilon_{23} = -\frac{\bar{s}_{32}}{\bar{s}_{22}}, \ \upsilon_{13} = -\frac{\bar{s}_{31}}{\bar{s}_{11}}, \ \upsilon_{12} = -\frac{\bar{s}_{21}}{\bar{s}_{11}}.$$

Three Chentsov's coefficients:

$$\mu_{23,31} = \frac{\bar{s}_{45}}{\bar{s}_{55}}, \ \mu_{23,12} = \frac{\bar{s}_{46}}{\bar{s}_{66}}, \ \mu_{31,12} = \frac{\bar{s}_{56}}{\bar{s}_{66}}.$$

Nine mutual influence coefficients:

$$\eta_{1,23} = \frac{\bar{s}_{14}}{\bar{s}_{44}}, \eta_{1,31} = \frac{\bar{s}_{15}}{\bar{s}_{55}}, \eta_{1,12} = \frac{\bar{s}_{16}}{\bar{s}_{66}},$$
$$\eta_{2,23} = \frac{\bar{s}_{14}}{\bar{s}_{44}}, \eta_{2,31} = \frac{\bar{s}_{15}}{\bar{s}_{55}}, \eta_{2,12} = \frac{\bar{s}_{16}}{\bar{s}_{66}},$$
$$\eta_{3,23} = \frac{\bar{s}_{14}}{\bar{s}_{44}}, \eta_{3,31} = \frac{\bar{s}_{15}}{\bar{s}_{55}}, \eta_{3,12} = \frac{\bar{s}_{16}}{\bar{s}_{66}}.$$

Moreover, the degree of anisotropy is now available by defining 9 independent symmetry criteria f_a, expressed in [%], reposing on the effective mechanical properties, as presented in the following. A criterion f_a is considered valid if its value, expressed in [%], respects the condition $f_a \leq 1\%$.

Two criteria on the Young's moduli:

$$f_1 = \frac{|E_3 - E_2|}{E_2}, f_2 = \frac{|E_1 - E_2|}{E_2}.$$

Two criteria on the shear's moduli:

$$f_3 = \frac{|G_{31} - G_{23}|}{G_{23}}, f_4 = \frac{|G_{12} - G_{23}|}{G_{23}}.$$

Two criteria on the Poisson's ratios:

$$f_5 = \frac{|\upsilon_{31} - \upsilon_{23}|}{\upsilon_{23}}, f_6 = \frac{|\upsilon_{12} - \upsilon_{23}|}{\upsilon_{23}}.$$

One criterion on the relationship between previous properties:

$$f_7 = \frac{\left| G_{23} - \frac{E_2}{2(1+\upsilon_{23})} \right|}{G_{23}}.$$

Two criteria on the Chentsov's and mutual influence coefficients sets μ and η, respectively:

$$f_8 = max(|\mu|), f_9 = max(|\eta|)$$

4 NUMERICAL RESULTS AT THE MESOSCOPIC SCALE

4.1 Convergence analyses

To validate the accuracy and effectiveness of the FE model of the RVE, convergence analyses on the RVE size and on the mesh size are realised on the equivalent elastic properties results while optimising the computational time. The study is realised in the case of the mean values of physical parameters on the whole range of distance to the pith R.
The details of these sensitivity analyses will be presented during the speech. In the case of the RVE size, for a supposed constant mesh size of $e_{size} = 0.5$mm for 3D element, an optimal RVE size of h = 8mm is selected which respect the condition for rectangular parallelepiped rings. Furthermore, this condition allows to superimpose the local coordinate cylindrical reference system to the local Cartesian reference system. In the case of the mesh size convergence, for a RVE size of h = 8mm, the optimal mesh size is constant and equal to $e_{size} = 1\text{mm} = h/8$. Here, the study is realised on the mean values of physical parameters for only the smaller growth rings at $R >$ 100mm. The computational time needed for 1 simulation is about t = 3.0 seconds.

4.2 Monte-Carlo Method

The Monte-Carlo (MC) method is commonly used to estimate the probabilistic distribution of simulation results and have already been used in the case of natural material [12]. In our specific case, for a RVE volume positioned at a certain distance to the pith R, the variability of physical parameters and mechanical properties at the microscopic scale induce uncertainty on the resulting effective properties at the mesoscopic scale, which can be assessed thanks to the MC method coupled with the numerical homogenisation technique. The probabilistic distribution is supposed to follow a normal distribution for the resulting elastic properties. The MC method applied in our study relies on four main steps.

• Step 1: The parametric FE model takes into consideration the variability of each input parameter, as presented in Section.2.
• Step 2: In the statistical domain, it is mandatory to obtain information on a given population by performing a random sampling. Its main purpose is to select a statistically representative number of samples of our studied population.
• Step 3: The homogenisation process is carried out on each sample to obtain the probabilistic distribution of the equivalent elastic properties at the upper scale at a given distance to the pith R.
• Step 4: Step 1-3 are repeated for some values of R in the range R ∈ [4,150]mm with an increment of 1mm. The number of samples n adequate in the case of our study has been estimated by studying the convergence of equivalent elastic properties mean and standard deviation of RVE volume over the whole range of R for different values of n. For the sake of brevity, this analysis is not presented here and will be discussed during the speech. The number of samples to achieve convergence is n = 250. Hence, the whole MC method takes approximately t_{tot}= 30 hours.

4.3 Numerical results for the effective properties.

In this section, the results of the numerical study are presented. To show the effectiveness of the proposed approach, a comparison between our numerical model and the analytical model of Reuss-Voigt over the range of interest R is accomplished. Furthermore, scientific literature data of interest are juxtaposed to the results as further comparison term. They are taken from various studies such as [15,16,24,25,26,27,28]. Over the whole range of R, only the criteria f_8 and f_9 are verified. Therefore, the homogenised material at the upper scale can be considered as an orthotropic material. For the sake of brevity, only the equivalent properties E_1 and G_{23} are presented in Figure 3.

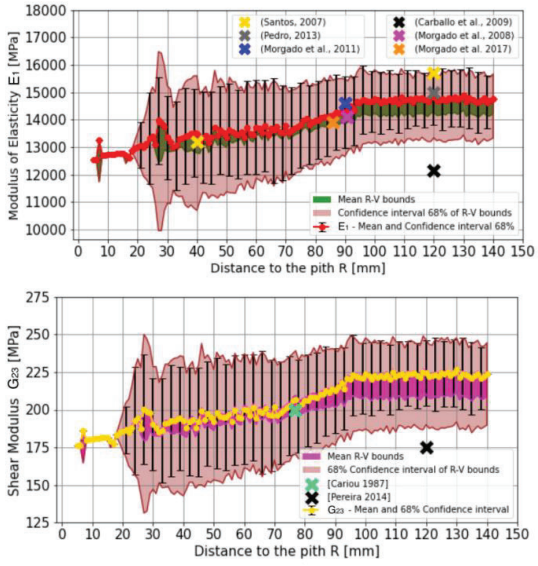

Figure 3: *Numerical results for the equivalent properties* $\boldsymbol{E_1}$ *and* $\boldsymbol{G_{23}}$ *over the whole range [5,140]mm versus experimental results.*

5 LAMELLAE PROPERTIES AT THE MACROSCOPIC SCALE

The purpose of this section is to obtain the equivalent mechanical properties of lamellae at the macroscopic scale. The lamellae are rectangular parallelepipeds of dimensions $A_1 = 500$mm, $A_2 = 95$mm, and $A_3 = 24$mm, along the X_1, X_2, and X_3 axis, respectively, of a global Cartesian reference system (O; X_1, X_2, X_3) defined at the centre of the log.
The lamellae and the RVE positions are defined by the position of their centre, respectively by the distances L, R, and the angle φ in the cylindrical reference system (O; L, R,T) with L the longitudinal axis, as illustrated in Figure 4.

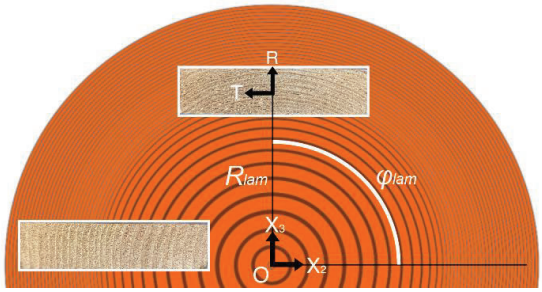

Figure 4: *Reference systems and position of the lamellae in the log.*

In Section 4, the equivalent properties of Pinus pinaster (Ait.) have been computed at the mesoscopic scale thanks to a homogenisation technique coupled with a stochastic approach. These properties are dependent only of the distance to the pith of the volumes R and are independent from the angle φ.
As the X_1 direction has no influence on the lamellae and cubes properties, we will consider only a section of dimensions $A_2 = 95$mm and $A_3 = 24$mm to describe the lamellae in the plane (O; X_2, X_3). To estimate the properties at the mesoscopic scale, we propose to discretise the lamellae as a combination of elementary sections with respect to their corresponding local orientation in the cylindrical reference system.
Finally, approximation methods resting on the utilisation of NURBS surfaces are used to compute the lamellae equivalent properties at the mesoscopic scale from the discretised mechanical properties found in Section 4.

5.1 Non-uniform rational basis-spline (NURBS) hyper-surfaces theory

This section gives a brief reminder of NURBS surfaces theory. These entities generalise the B-Splines surfaces, which generalise the Bézier surfaces [29]. Originally employed in Computer Aided Design (CAD) in the 1990's, these entities are now used in multiples domains, such as topology optimisation [32, 33, 34], shape optimisation [31, 38], anisotropy field optimisation for variable stiffness composites [36, 37], and surrogate model generation [30].

https://doi.org/10.52202/069179-0062

In this work, the NURBS surfaces entities are used as response surfaces (or surrogate models). Their aim is to fit the discrete mechanical properties of a material section or Target Points (TP) to homogenise and render a proper physical interpretation over the entire section. In other words, NURBS surfaces are used as approximation surfaces to fit the TP scalar data identified by their coordinates (X_2, X_3).

NURBS surfaces are used to approximate a model $M : \mathbb{R}^n \mapsto \mathbb{R}^m$, where $n = 2$ and $m = 12$ correspond to the dimensions of (X_2, X_3) coordinates, and to the dimensions of the set of desired mean and standard deviation mechanical properties extracted from the numerical study of Section 4, respectively. In the present case, these properties are the Young's moduli, the shear moduli and the corresponding standard deviations.
The parametric explicit form of each coordinate of a NURBS entity with only two input parameters reads:

$$s_b(u_2, u_3) = \frac{\sum_{i_2=0}^{n_2} \sum_{i_3=0}^{n_3} N_{i_2,p_2}(u_2)\, N_{i_3,p_3}(u_3) \omega_{i_2,i_3} P_{b,i_2,i_3}}{\sum_{i_2=0}^{n_2} \sum_{i_3=0}^{n_3} N_{i_3,p_3}(u_2)\, N_{i_3,p_3}(u_3) \omega_{i_2,i_3}} \tag{10}$$

with $s_b(u_2, u_3)$ the NURBS output b-mechanical property $(b \in [1, m])$ evaluated at the normalised input coordinates $(u_2 \in [0,1], u_3 \in [0,1])$. $n_k + 1 \;\; (k = 2,3)$is the number of control points (CPs) along the u_k parametric direction. ω_{i_2,i_3} corresponds to the weight assigned to the CP of indices i_2, i_3 . In this case, it is taken equal to 1 for every CP. P_{b,i_2,i_3} represents the $(n_2 + 1)(n_3 + 1)$ CPs coordinates. $N_{i_k,p_k}(u_k) \;\; (k \in [2,3])$ are the basis functions of degree p_k (equal to 2 in our study) and are evaluated recursively with the Cox de Boor algorithm, based on Bernstein's polynomials [35]. For more information on this matter, the interested reader is referred to [29].
Each timber section is discretised with $N_{TP} = N_2 N_3$ TPs and the number of CPs of the NURBS entity vary as $N_{CP} = \delta\, N_{TP}$. Employing the surface fitting algorithm of [30], the CPs drive the NURBS surface across each output to obtain the distribution of the equivalent elastic properties of the lamellae at the macroscopic scale.

5.2 Sensitivity of the results to the number of target points and control points.

Firstly, a NURBS of degree 3 and $\delta = 1/4$ is applied to the input mechanical properties at the mesoscopic scale computed in Section 4 to smoothen the input curves. For the sake of conciseness, this interpolation process is not presented in this paper and will be presented during the speech.
To validate the interpolation method to compute the lamellae effective properties at the mesoscopic scale, convergence analyses must be made in terms of number of TPs and CPs. As the section geometry is defined in a Cartesian reference system, the TP and CP are also defined in the same reference system and are distributed uniformly across the directions X_2 and X_3.

The results of the sensitivity analysis allow to achieve convergence for a number of TPs equal to $N_{\mathrm{TP}} = 75 \times 30$ for all typologies of lamellae studied.
Regarding the number of CPs, the convergence is achieved with $\delta = 2/3$ to maximise the coefficient of correlation.
The precision of the NURBS surfaces is evaluated by comparing the relative differences between input and output values (a set of TPs different from the one used to determine the approximating NURBS entity). As the relative difference is under 2% for every mechanical properties, the interpolation method is validated.
Finally, defining the TPs and CPs in a Cartesian reference system induce variability of the output properties according to φ (should depend solely on the distance to the pith R) and is evaluated to 5% for a constant value of R.

5.3 Lamellae properties at the macroscopic scale

The NURBS entities are used to compute the equivalent properties of lamellae of two typologies. The first typology is a lamella whose centre is positioned at $R_1 = 50$mm and $\varphi_1 = 0$ while the second is positioned at $R_1 = 80$mm and $\varphi_1 = \pi/2$ and are presented in Figure 5. Only the input data (TP) and the output NURBS effective properties for the mean longitudinal modulus are presented for the sake of brevity.

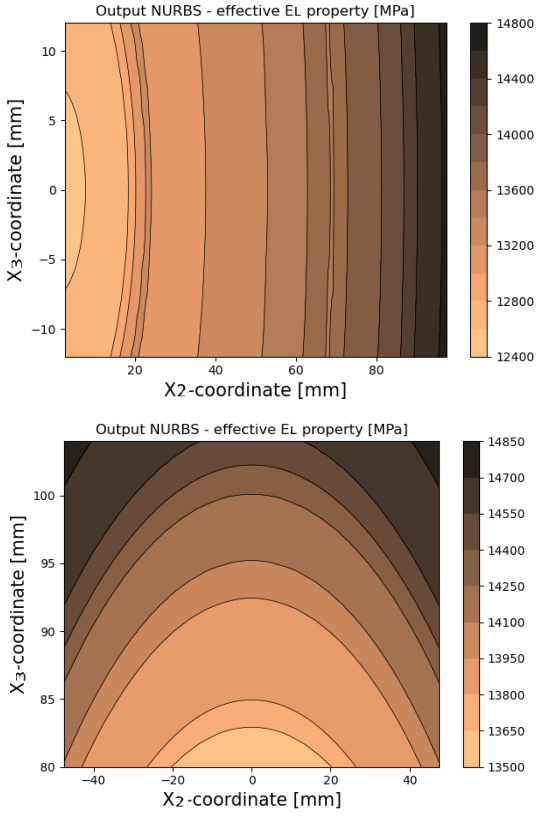

Figure 5: *Output NURBS effective properties (longitudinal modulus) of two typologies of lamellae at the macroscopic scale.*

6 CONCLUSIONS

Effective elastic properties of lamellae of Pinus pinaster (Ait.) at the macroscopic scale have been computed. The model took into account the several sources of variability and their propagation across the scales.

The scientific literature allowed to propose several models of elastic behaviour dependent on the density for the initial and final wood at the microscopic scale.

Numerical composite homogenisation techniques have been used in the case of elementary volumes considered as lamellar composites of initial and final woods.

The "Strain Homogenization Technique" has been used on the RVE to homogenise the effective properties at the mesoscopic scale (including the associated variability).

The lamellae are then discredited into several data reference. An approximation method reposing on the use of NURBS entities has been used to model the elastic behaviour of some configurations of lamellae.

This work focuses on computing homogenised properties to be used for Pinus pinaster (Ait.) instead of the classical softwood properties classically chosen.

These properties adapted to the case of Pinus pinaster (Ait.) can be imported into a model representing multiples configurations of glulam at the macroscopic scale by taking into account the finger-jointing and gluing of the components.

The next step would be to model the impact of grain angle, conical angle, micro-fibril angle, reaction wood, log shape, and centred pith on the results as additional sources of variability to better represent the reality of wood growth.

REFERENCES

[1] IPCC, (2018): Global Warming of 1.5°C.An IPCC Special Report on the impacts of global warming of 1.5°C above pre-industrial levels and related global greenhouse gas emission pathways, in the context of strengthening the global response to the threat of climate change, sustainable development, and efforts to eradicate poverty [Masson-Delmotte, V., P. Zhai, H.-O. Pörtner, D. Roberts, J. Skea, P.R. Shukla, A. Pirani, W. Moufouma-Okia, C. Péan, R. Pidcock, S. Connors, J.B.R. Matthews, Y. Chen, X. Zhou, M.I. Gomis, E. Lonnoy, T. Maycock, M. Tignor, and T. Waterfield (eds.)]. In Press

[2] Vidal, M. (2016). Optimisation des stratégies d'amélioration génétique du pin maritime grâce à l'utilisation de marqueurs moléculaires [Phdthesis, Université de Bordeaux]. https://tel.archives-ouvertes.fr/tel-01359191

[3] Ormarsson, S., Dahlblom, O., Petersson, H. (2000). A numerical study of the shape stability of sawn timber subjected to moisture variation. Wood Science and Technology. 34. 207-219. 10.1007/s002260000042.

[4] Lasserre, B. (2000). Modélisation thermo-hygro-mécanique du comportement différé de poutres de structure en bois [These de doctorat, Bordeaux 1]. http://www.theses.fr/2000BOR10561

[5] Clouet, B. (2014). Comportement hydromécanique d'assemblages bois collés à l'état vert : Approches expérimentale et numérique [These de doctorat, Bordeaux]. https://www.theses.fr/2014BORD0036

[6] Guitard, D. (1987). Mécanique du matériau bois et composites / Préface de Polge H.. Cépaduès-Editions.

[7] Grazide, C. (2014). Une modélisation de la résistance en flexion du pin maritime utilisé en construction [PhD Thesis, Université de Bordeaux]. https://tel.archives-ouvertes.fr/tel-01176734

[8] Berthier, B., A.D., Kokutse, A. Stokes, T. Fourcaud (2001). Irregular Heartwood Formation in Maritime Pine (Pinus pinaster Ait.): Consequences for Biomechanical and Hydraulic Tree Functioning. Annals of Botany, 87(1):19–25.

[9] Moreau, J. (2010). Impact de pratiques sylvicoles intensives sur les proprietés du bois de pin maritime. Phd thesis, Université de Bordeaux 1. URL: https://www.theses.fr/2010BOR14200

[10] Nicholls, J.W.P., H.E., Dadswell, and D.H., Perry (1963). Assessment of wood qualities for tree breeding. II. In Pinus Pinaster Ait. from Western Australia. Silvae Genet, 12(4):105–110.

[11] Gaspar, M.J., J., Louzada, M., Silva, A., Aguiar, and M.H., Almeida (2008). Age trends in genetic parameters of wood density components in 46 half-sibling families of Pinus pinaster. Canadian Journal of Forest Research, 38(6):1470–1477.

[12] Delucia, .M., A., Catapano, M., Montemurro, J., Pailh´es (2020). A stochastic approach for predicting the temperature-dependent elastic properties of cork-based composites. Mechanics of Materials, 145103399.

[13] Louzada, J.L.P.C. (2003). Genetic correlations between wood density components in Pinus pinaster Ait. Annals of Forest Science, 60(3):285–294.

https://doi.org/10.52202/069179-0062

[14] Kasal, B. (2004). Chapter : Wood formation and properties — Mechanical Properties of Wood. In book: Encyclopedia of Forest Sciences Copyright: Academic Press. pp.1815-1828
[15] Santos, J. (2007). Estudo de Modelos e Caracterização do Comportamento Mecânico da Madeira. PhD thesis, UNIVERSIDADE DO MINHO.
[16] Cariou, J.-L. (1987). Caractérisation d'un matériau viscoélastique anisotrope: le bois. PhD thesis, Universit´e Bordeaux I. OCLC: 489807750.
[17] Pereira, J.L. (2005). Comportamento mecânico da madeira em tracção nas direcões de simetria material. Master's thesis, Universidade de Tràs-os-Montes e Alto Douro, Vila Real, Portugal.
[18] Lahna, F. (1983). Mécanique de la rupture des matériaux orthotropes-Application au bois. Phdthesis, Université de Bordeaux 1. URL: http://www.theses.fr/2010BOR14200.
[19] Xavier, J.C., N.M,. Garrido, M., Oliveira, J.L., Morais, P.P., Camanho, F., Pierron (2004). A comparison between the Iosipescu and off-axis shear test methods for the characterization of Pinus Pinaster Ait. Composites Part A: Applied Science and Manufacturing, 35(7-8):827–840.
[20] FPL (2010). Wood Handbook, Wood as an Engineering Material. General Technical Report FPLGTR-190, U.S. Departement of Agriculture, Forest Service, Madison.
[21] Barbero, E. J. (2007). Finite Element Analysis of Composite Materials. CRC Press.
[22] Vieira, J., Campelo, F., Rossi, S., Carvalho, A., Freitas, H., & Nabais, C. (2015). Adjustment Capacity of Maritime Pine Cambial Activity in Drought-Prone Environments. PLOS ONE, 10(5), e0126223. https://doi.org/10.1371/journal.pone.0126223
[23] Catapano,. A., J., Jumel (2015). A numerical approach for determining the effective elastic symmetries of particulate-polymer composites. Composites Part B: Engineering, 78227–243.
[24] Pereira, J., J., Xavier, J., Morais, J., Louzada (2014). Assessing wood quality by spatial variation of elastic properties within the stem: Case study of Pinus pinaster in the transverse plane1. Canadian Journal of Forest Research, 44:107–117. Plomion, C., C., Pionneau, J., Brach, P., Costa.
[25] Pedro, J. (2013). Avaliação destrutiva e não destrutiva de elementos retangulares de madeira de pinho bravo. Master's thesis, Faculdade de Ciencias e Tecnologia da Universidade de Coimbra, Portugal.
[26] Morgado, T.F.M., J.S., Machado, A.M.P.G., Dias, H., Cruz, J.N.A., Rodrigues (2011). Caracteristicas mecânicas et classifição da madeira de secção circular de Pinheiro Bravo CIMAD 11 -1°Congresso Ibero-LatinoAmericano da Madeira na Construção, 7-9/06-2011, Coimbra, Portugal.
[27] Morgado, T.F.M., A.M.P.G., Dias, J.S., Machado, J.H.J.O., Negrao, A., Marques (2017). Grading of Portuguese Maritime Pine Small-Diameter Roundwood. Journal of Materials in Civil Engineering, 29(2):04016209.
[28] Carballo, J., E., Hermoso, J.I., Fernandez-Golfin (2009). Mechanical properties of structural maritime pine sawn timber from Galicia (Pinus pinaster Ait. ssp.atlantica) Investigacion Agraria: Sistemas y Recursos Forestales,18(2):152–158.
[29] Les Piegl and Wayne Tiller. The NURBS books. Springer-Verlag, New York, NY, USA, second edition, 1996.
[30] Yohann Audoux, Marco Montemurro, and Jérôme Pailhès. A metamodel based on non-uniform rational basis spline hyper-surfaces for optimisation of composite structures. Composite Structures, 247 :112439, 2020
[31] Giulia Bertolino, Marco Montemurro, and Giorgio Pasquale. Multi-scale shape optimisation of lattice structures: an evolutionary-based approach. International Journal for Interactive Design and Manufacturing (IJIDeM), 12 2019.
[32] Giulio Costa, Marco Montemurro, and Jérôme Pailhès. Minimum length scale control in a nurbsbased simp method. Computer Methods in Applied Mechanics and Engineering, 354 :963-989, 2019.
[33] Thibaut Rodriguez, Marco Montemurro, Paul Le Texier, and Jérôme Pailhès. Structural displacement requirement in a topology optimization algorithm based on isogeometric entities. Journal of Optimization Theory and Applications, 184 :250-276, 2020.
[34] Giulio Costa, Marco Montemurro, and Jérôme Pailhès. Nurbs hyper-surfaces for 3d topology optimization problems. Mechanics of Advanced Materials and Structures, 28(7) :665-684, 2021.
[35] Carl De Boor. On calculating with B-Spline. Journal of Approximation theory, 6(1) :50-62, 1972.
[36] Marco Montemurro and Anita Catapano. On the effective integration of manufacturability constraints within the multi-scale methodology for designing variable angle-tow laminates. Composite Structures, 161 :145-159, 02 2017.
[37] Marco Montemurro and Anita Catapano. A general b-spline surfaces theoretical framework for optimisation of variable angle-tow laminates. Composite Structures, 209 :561-578, 2019.
[38] Marco Montemurro, Anita Catapano, and Dominique Doroszewski. A multi-scale approach for the simultaneous shape and material optimisation of sandwich panels with cellular core. Composites Part B : Engineering, 91 :458-472, 2016.